



## Influence of polycation/cation competition on the aggregation threshold of magnetic nanoparticles

Mesut Demirelli, Véronique Peyre, Juliette Sirieix-Plénet, Natalie Malikova,  
Jérôme Fresnais

### ► To cite this version:

Mesut Demirelli, Véronique Peyre, Juliette Sirieix-Plénet, Natalie Malikova, Jérôme Fresnais. Influence of polycation/cation competition on the aggregation threshold of magnetic nanoparticles. Colloids and Surfaces A: Physicochemical and Engineering Aspects, 2020, pp.125876. 10.1016/j.colsurfa.2020.125876 . hal-03058032

**HAL Id: hal-03058032**

**<https://hal.science/hal-03058032>**

Submitted on 11 Dec 2020

**HAL** is a multi-disciplinary open access archive for the deposit and dissemination of scientific research documents, whether they are published or not. The documents may come from teaching and research institutions in France or abroad, or from public or private research centers.

L'archive ouverte pluridisciplinaire **HAL**, est destinée au dépôt et à la diffusion de documents scientifiques de niveau recherche, publiés ou non, émanant des établissements d'enseignement et de recherche français ou étrangers, des laboratoires publics ou privés.

# Influence of polycation/cation competition on the aggregation threshold of magnetic nanoparticles

Mesut Demirelli, Véronique Peyre, Juliette Sirieix-Plénet, Natalie Malikova, Jérôme Fresnais

Sorbonne Université, CNRS, Laboratoire de Physico-chimie des Electrolytes et Nanosystèmes Interfaciaux, PHENIX - UMR 8234, F-75252 Paris cedex 05, France.

## ABSTRACT

Precise control of the aggregation of magnetic nanoparticles in aqueous environment is a key to their successful application in the biological and medical fields. We investigate here the critical aggregation threshold of PAA-coated maghemite nanoparticles in aqueous solution, in the presence of ionenes, polycations with a regular, tunable and pH-insensitive chain charge density, and a variety of ammonium-based salts. Aggregation of the nanoparticles is followed by a combination of dynamic light scattering and light absorbance measurements, along a dilution pathway from initially dispersed systems at high salt concentration (3M). The position of the aggregation threshold, or critical salt concentration, is found to depend on two parameters: volume of the salt cation ( $V_{\text{cation}}$ ) and volume of the charged monomer unit of the polycation ( $V_{\text{mono}}^+$ , reflecting the polycation charge density). Combining these two parameters, a master curve emerges, showing that the critical salt concentration follows in a linear fashion the ratio of the above two volumes,  $V_{\text{cation}}/V_{\text{mono}}^+$ . Interpreted within the theory of Collins and coworkers, the master curve is a clear demonstration of the importance of local ion-pairing in governing the stability of the system, which remains unaccounted for in the continuum electrostatic theories attempting to describe polyelectrolyte complex formation. Moreover, such a master curve provides a very simple rule for the control of interactions between charged polyelectrolytes moderated by salts.

**KEYWORDS:** Magnetic Nanoparticles; Polyelectrolyte; electrostatic complexation; Hofmeister series; iron oxide; aggregation; ammonium cations, screening, light scattering

## INTRODUCTION

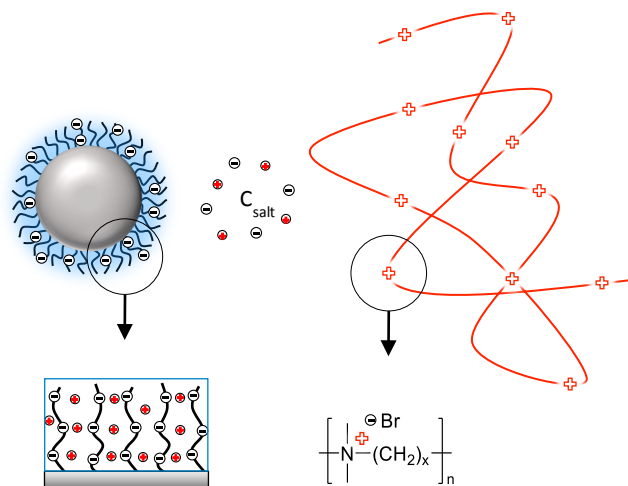
Magnetic nanoparticles have many potential applications in medicine as nanoheaters<sup>1</sup>, nanoplateforms for active molecule transport<sup>2</sup>, and contrast agents in magnetic resonance imaging<sup>3</sup>. In some specific cases, the small size of the nanoparticles is a strength due to the magnetic monodomain they contain<sup>4</sup>, but this small size (few nanometres in diameter) makes them difficult to manipulate. As such, controlled aggregates can be a way to combine the superparamagnetic properties of single nanoparticles and low magnetic fields needed to manipulate them<sup>5</sup>. Aggregates based on electrostatic complexation are promising in this sense, as this assembly process is highly tunable<sup>6,7,17,18,22-26</sup> and allows modulating not only the structure/density of the final aggregate but also its region of stability.

Maghemite nanoparticles (NP)<sup>14-17</sup>, and their significantly increased colloidal stability through electrosteric repulsion<sup>18,19</sup> due to a polymer coating<sup>18,20,21</sup> such as poly (acrylic) acid (PAA), have been extensively studied. One route for tuning the stability of coated maghemite nanoparticles (CNPs) in aqueous solution is the addition of oppositely charged polymer chains. In the case of PAA-coated particles at high pH, these polymer chains are polycations (PCs). The underlying phenomenon is the electrostatic complexation between the polyanions forming the NP coating and the free polycations: at low ionic strength, PAA-coated maghemite nanoparticles in the presence of polycations form clusters and aggregates, as a result of attractive electrostatic forces,<sup>22</sup> while the same mixtures show remarkable stability at high ionic strength (salt concentrations of 1-3 mol L<sup>-1</sup>), owing to electrostatic screening.<sup>5,22</sup> One way of exploring the transition from a dispersed to an aggregated state of PAA-coated maghemite particles, in the presence of polycations, is to gradually decrease the ionic strength through a dilution pathway.<sup>22</sup> Several groups have shown measurements of this transition for systems with different types of coated nanoparticles<sup>17-21</sup>, which occurs at what is referred to as the critical salt concentration. Ion valence is of outmost importance, however moving from monovalent to multi-valent ions usually changes the entire picture. In other words, monovalent and multivalent ions cannot be considered in a continuous scheme. Addition of multivalent salts into dispersions of PAA-coated nanoparticles leads to a rapid and irreversible aggregation of the particles, even in the absence of polycations. Thus, we consider here only monovalent salts and polycations with one charge per monomer.

Understanding electrostatic complexation of oppositely charged polyelectrolytes (PEs) remains a formidable task. These systems are strongly correlated<sup>26</sup> and described by a large number of parameters.<sup>27-30</sup> Some of the parameters are easy to quantify (polymer concentration, charge density, mixing ratio, molecular weight), while for others an empirical classification has to suffice for now. Among the latter falls clearly the chemical specificity of the ionic groups involved (not only those on the polymer chains, but also the surrounding salt ions) as embodied by the Hofmeister

series<sup>31–33</sup>. This remains to date an empirical ordering of cations/anions and reflects their relative effect on the stability of organic (biological) macromolecules and inorganic colloids in water. Theoretical approaches to PE complex formation span a wide conceptual range. Firstly, we may distinguish those stemming from continuum electrostatics, which originate in the classical Voorn-Overbeek (VO) mean-field model<sup>34–36</sup>, secondly, those based on liquid state theory allowing a more explicit description of charge-charge correlations<sup>37</sup> and, lastly, those departing from local phenomena of ion pairing, counterion release and solute-solvent interactions<sup>38–40</sup>. The latter approach is the more natural for consideration of the chemical specificity of the ionic groups involved.

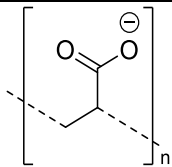
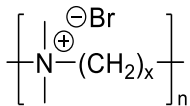
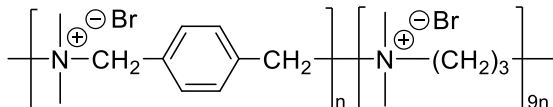
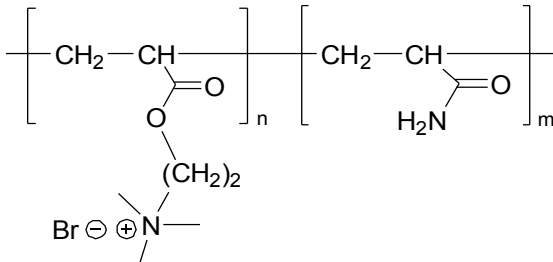
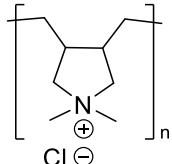
A great deal of attention has been paid to evaluate the relative weight of the enthalpy and entropy contributions in the process of PE complex formation. Currently, the majority of studies points towards the process being entropically driven, stemming from the release of the polyelectrolyte counterions<sup>26,27,38,39,41,42</sup>. Most recently, Schlenoff and collaborators have used isothermal titration calorimetry to systematically evaluate the interactions between oppositely charged polyelectrolytes<sup>33,34</sup>. They have confirmed that the electrostatic complexation (either coacervation or precipitation) is entropically driven, not only due to the release of counterions but also due to the restructuring of the solvent water molecules. They also provided a hybrid model where both entropic effect and the Donnan pressure can be considered to highlight the role of counterion release in the process of complex formation<sup>39</sup>, through the use of different anions along the Hofmeister series. They were able to establish that the equilibrium constant of the polyelectrolyte pairing was dependent on the nature of the added ions (chaotropic or kosmotropic). The specificity of the salt ion had an impact on the enthalpic component of the complex formation, while the entropic component was still dominated by the release of counterions and water molecules.



**Figure 1.** Schematic representation of the system: spherical maghemite NPs<sup>43</sup> with an anionic PAA brush and polycations, ionenes.<sup>44</sup> PAA is strongly complexed onto NPs and, at pH=9, leads to a brush layer at full ionisation of the carboxylate groups of PAA.<sup>18</sup> Ethylammonium cations and bromide anions are, respectively, the counterions of PAA and ionenes. Added salt is present at a concentration  $c_{salt}$ .

In this study we investigate the role of salt ions in screening the interactions between PAA coated maghemite nanoparticles and ionene polycations. Our focus is on the PAA coated maghemite nanoparticles and we work under conditions of excess of ionene polycations. We seek to tune the location of the dispersed-aggregated transition, represented by the critical salt concentration,  $[Salt]_{critical}$ . We start with stable nanoparticle dispersions at a high ionic strength ( $c_{salt}=3 \text{ mol.L}^{-1}$ ) and use the aforementioned dilution pathway. As the nanoparticle polymer coating is negatively charged under the chosen experimental conditions (pH=9), the primary role in tuning the transition is that of the salt cations and the polycations, as opposed to any anions present. As shall be seen, we have clear evidence that for a common anion ( $Br^-$ ), two different ammonium-based salt cations lead to a very different nanoparticle aggregation threshold. The tuning of the aggregation threshold is thus achieved via a combination of two parameters: (i) the charge density of the ionene polycations and (ii) the nature of the salt cation. The salt cations, as well as the ionene polycations, are all based on charged ammonium centres. Ionene polycations are strong polyelectrolyte chains and thus possess a permanent charge, which is pH-insensitive. Additionally, the interest behind ionene polycations is the strict regularity and possibility of exact tuning of their linear charge density<sup>44,45</sup>. We arrive at a simple relationship for the tuning of the particle aggregation threshold, which is based on the relative volume of the salt cations and the charged monomer units of ionene polycations.

**Table 1.** Abbreviations, full names and molecular structures of the polyanion PAA and polycations studied.

Abbreviation	Full Name	Structure
PAA <sup>-</sup>	Poly (acrylic acid)	
x-ionene <sup>46,47</sup> (x=3, 6, 9)	x, x-ionene	
3- Bz	3,3-p-BzBr (90:10)	
PTEA-PAM <sup>22</sup>	Poly (trimethylammonium ethyacrylate) <sub>11</sub> κ- <i>b</i> -poly (acrylamide) <sub>30K</sub>	
PDADMAC <sup>22</sup>	Poly (diallyldimethylammonium chloride)	

## 1. EXPERIMENTAL

### 1.1. Materials

The following materials were purchased and used without further purification.

Tetraethylammonium bromide (TEABr, > 99 wt % Fluka Chemie); tetramethylammonium bromide (TMABr, > 98 wt %, Sigma-Aldrich); ammonium chloride (NH<sub>4</sub>Cl, Prolabo); iron (II) chloride (FeCl<sub>2</sub>\*4H<sub>2</sub>O, AnalaR Normapur, VWR); iron (III) chloride (FeCl<sub>3</sub>\*6H<sub>2</sub>O, VWR); iron (III) nitrate (Fe(NO<sub>3</sub>)<sub>3</sub>\*9H<sub>2</sub>O, technical, VWR); N, N, N', N'-Tetramethyl-1,3-propanediamine (≥99 wt %, Sigma-Aldrich), 1,4-bis-bromomethyl-benzene (≥98 wt %, Sigma-Aldrich); N, N, N', N'-tetramethyl-1,6-hexanedi-amine (99 wt %, Sigma-Aldrich), 1,3-dibromopropane (99 wt %, Sigma-Aldrich); 1,6-dibromohexane (96 wt %, Sigma-Aldrich); 1,9-dibromononane (97 wt %, Sigma-Aldrich); Dimethylamine hydrochloride (98 wt %, Sigma-Aldrich); poly (acrylic acid sodium salt) (PAA Na,

average  $M_w = 2100$  g/mol, Sigma-Aldrich); tetrahydrofuran ( $\geq 99.9$  wt %, AnalaR Normapur, VWR); methanol (99.8 wt %, Sigma-Aldrich); acetone (technical, AnalaR Normapur, VWR); chloroform ( $\geq 99$  wt %, CARLO ERBA); diethyl ether (99.8 wt %, AnalaR Normapur); dimethylformamide (DMF, 99.8 wt %, Sigma-Aldrich), hydrochloric acid (HCl, 37 wt % aqueous solution, AnalaR Normapur); nitric acid ( $\text{HNO}_3$ , 68 wt % aqueous solution, AnalaR Normapur, VWR); sodium hydroxide (NaOH pellets, 98 wt %, Acros Organics); ethylamine ( $\text{EtNH}_2$  70 wt % aqueous solution, Merck); distilled water.

### 1.1.1 Iron Oxide Nanoparticles

The synthesis of bare magnetic nanoparticles (BNP, maghemite,  $\gamma\text{-Fe}_2\text{O}_3$ ) through coprecipitation of  $\text{Fe}^{\text{II}}$  and  $\text{Fe}^{\text{III}}$  in water was established by R. Massart.<sup>14</sup> Their size polydispersity was reduced by size sorting through selective flocculation of the larger particles by increase of the ionic strength.<sup>16</sup> The nanoparticles were characterised by Transmission Electron Microscopy (TEM). The picture analysis showed a log-normal size distribution of median diameter  $d_0 = 7$  nm and a polydispersity index  $\sigma = 0.2$  (SI 1). Small angle X-ray scattering results are reported in the Supporting Information (SI-2) and confirmed the particle size determined by the former methods.

The concentration of maghemite particles was consistently determined via UV-visible spectroscopy (Section 2.2.2) and atomic absorption spectroscopy (Section 2.2.3). For the first method, a master curve (500-700 nm, Supporting Information, SI 3) was used for dilutions in distilled water and for the second the NP were dissolved in concentrated HCl.

### 1.1.2 Coating of NP

A coating of poly (acrylic acid) around the maghemite nanoparticles was performed via electrostatic complexation following the precipitation-redispersion process.<sup>20</sup> The precipitation step is conducted at pH 1.5. During the redispersion step, ethylamine (7 wt %) is used to increase the pH to 9.0, ethylammonium is the counterion for the anionic carboxylate groups of PAA. The PAA-coating is irreversible and stays in place between pH 1.5 and 10.0. The  $\text{pK}_a$  of PAA is 4.5<sup>48,49</sup>, at pH below 4.5 the functional groups in the polymer chain are predominantly undissociated, while at pH above 4.5 polyanion (PA) dissociation increases and reaches full dissociation close to pH 9.0. Therefore, the experiments involving CNP were carried out at a pH = 9.0. The hydrodynamic diameter of these particles was determined at 39 nm via DLS. The density of PAA on the nanoparticle surface is 2 chains per  $\text{nm}^2$ .<sup>18</sup>

### 1.1.3 Ionenenes

The synthesis and the characterisation in terms of chain length and charge density of 3-, 6- and 9-*ionene* were previously reported by Malikova et al.<sup>44,50</sup>

For the synthesis of 3-Bz, N, N, N', N'-tetramethyl-1,3-propanediamine (20 mmol), 1,3-dibromopropane (18 mmol) and 1,4-bis-bromomethyl-benzene (2 mmol) were added into DMF (20 mL) in a round bottom flask. The reaction mixture was stirred and heated at 80 °C. When white precipitate appeared, 10 mL of water was added to the mixture to ensure the solubility of the components. The heating was maintained for 50h. After removal of solvents under reduced pressure, the residual product was dissolved in water and washed with chloroform 3 times. The aqueous phase was collected and the water removed via lyophilisation to give a white solid (80%). <sup>1</sup>H NMR (D<sub>2</sub>O, 300 MHz,)  $\delta$  (ppm) 2.37 (br, *n*.2H, -N<sup>+</sup>-CH<sub>2</sub>-CH<sub>2</sub>-CH<sub>2</sub>-N<sup>+</sup>), 3.18 (s, *n*.12H, CH<sub>3</sub>N<sup>+</sup>), 3.49 (t, *J*=8,1 Hz, 4H, *n*.2H, -N<sup>+</sup>-CH<sub>2</sub>-CH<sub>2</sub>-CH<sub>2</sub>-N<sup>+</sup>), 4.61 (s, 4H, N<sup>+</sup>-CH<sub>2</sub>-C<sub>H</sub>arom), 7.66 (s, 4H<sub>arom</sub>),

The polycations for this study are summarised in Table 1. Based on the structures of these PC and their molar volumes listed by Fedors<sup>51</sup>, the following charge density classification is made: 3-ionene > 3-Bz > PDADMAC > 6-ionene > PTEA-PAM > 9-ionene (SI 4).

#### 1.1.4 Synthesis of EAN

Ethylammonium nitrate (EAN) was synthesised according to procedures described previously.<sup>52,53</sup> Equimolar quantities of nitric acid (68 wt % aqueous solution) in a dropping funnel was added slowly to ethylamine (70 wt % aqueous solution) in a cooling bath at -15 °C. After the completion of addition, some excess ethylamine is added to reach basic pH and ensure completion of the reaction. The excess ethylamine is then eliminated under reduced pressure. The elimination of the water was achieved via lyophilisation. The residual water content was determined by Karl Fischer coulometric titration to give less than 0.4 wt %. The obtained ionic liquid is a viscous, odourless and transparent fluid with a pH 7.5, measured by the same method as in ref<sup>54</sup>.

### 1.2 Sample Preparation

**In aqueous solution:** The CNP-PC complexes were obtained by mixing stock solutions prepared at the same weight concentration (0.05 wt %) and the same pH (pH 9.0). The mixing of the two initial solutions was characterised by the charge ratio  $Z = Z^+/Z^-$ , where  $Z^+$  is the total number of positive charges of the PC in solution and  $Z^-$  is the total number of negative charges of the CNPs in solution.<sup>22</sup>

**In aqueous salt solution:** The individual stock solutions of CNPs and ionenes were prepared at the same weight concentration (0.5 wt %) and pH (pH 9.0) in 3 mol L<sup>-1</sup> aqueous salt solution, the molar



volumes of salts were included in the calculations of sample preparation (SI 4). The two initial solutions were mixed at a charge ratio  $Z = Z^+/Z^-$ .

**Dilution:** For the dilution process, distilled water was added to the CNP-PC mixtures stepwise. The concentration determination of well-dispersed CNPs was followed by UV-absorption spectroscopy (See Section 2.2.2). The size of the objects was determined by dynamic light scattering (See Section 2.2.1). Note that the measured  $[\text{Salt}]_{\text{critical}}$  values were independent of the initial concentrations of CNPs in stock solutions between 0.05 and 0.5 wt %.

### 1.3 Techniques

#### 1.3.1 Dynamic Light Scattering

Dynamic light scattering (DLS) measurements were performed with a MALVERN NanoZS (Malvern Instruments), at  $\lambda = 632$  nm and backscattering detection at angle  $\theta = 170^\circ$ . An autocorrelation function is determined by measurements of intensity at different times. The autocorrelation functions of the scattered light are interpreted by using the peaks of the cumulants (Z-average) in order to determine the diffusion coefficient. For this procedure, we approximated that the refractive indices of solutions remained unchanged during the dilution procedure.

The diffusion coefficient  $D$  under non-interacting conditions is related to the hydrodynamic radius  $R_H$  through the Stokes-Einstein equation:

$$D = \frac{k_B T}{6\pi\eta R_H} \quad (1)$$

where  $k_B$  is the Boltzmann constant,  $\eta$  the solvent viscosity and  $T$  the absolute temperature, all experiments were conducted at 298 K.

For the determination of hydrodynamic diameter in aqueous salt solutions, the viscosities of stock salt solutions from 3 to 0 mol L<sup>-1</sup> were measured (SI 5 and SI 6) and applied to the size determination via the Stokes-Einstein Equation (Equation 1).

#### 1.3.2 UV-visible-Absorption Spectroscopy

The measurements were conducted on an Avantes Avaspec 2048/Avalight DHC UV-Visible spectrometer. This technique is a simple and quick method and allows to quantitatively determine the concentration for solely well-dispersed nanoparticles solutions by using a master curve from 500 to 700 nm (SI 3) and determine the transition from a dispersed to an aggregated state (SI 7).

### 1.3.3 Atomic Absorption Spectroscopy (AAS)

The iron concentration of samples was determined by measurements of iron absorbance by Atomic Absorption Spectroscopy (AAS) on a Perkin-Elmer PinAAcle 500 instrument, after the dissolution of NP in concentrated hydrochloric acid and adapted dilutions. The expressed iron concentration  $[Fe]$  in  $\text{mol L}^{-1}$  converts to the volume fraction using the molar weight and density of maghemite as follows:<sup>17,55</sup>

$$\phi (\text{vol}\%) = 1.577 [Fe] \quad (2)$$

The concentration determination was made both via UV-Absorption and AAS and gave identical results. For reasons of simplicity, rapidity and convenience of the method, UV-absorption was used during dilutions.

### 1.3.4 Nuclear Magnetic Resonance

$^1\text{H}$  NMR spectra were recorded on a Bruker Advance 300 MHz spectrometer in  $\text{D}_2\text{O}$ . The following abbreviations were used to explain the multiplicities: s = singlet, d = doublet, t = triplet, br = broad.

## 2 RESULTS AND DISCUSSION

### 2.1 Coated maghemite nanoparticles in salty aqueous solutions in the absence of polycations

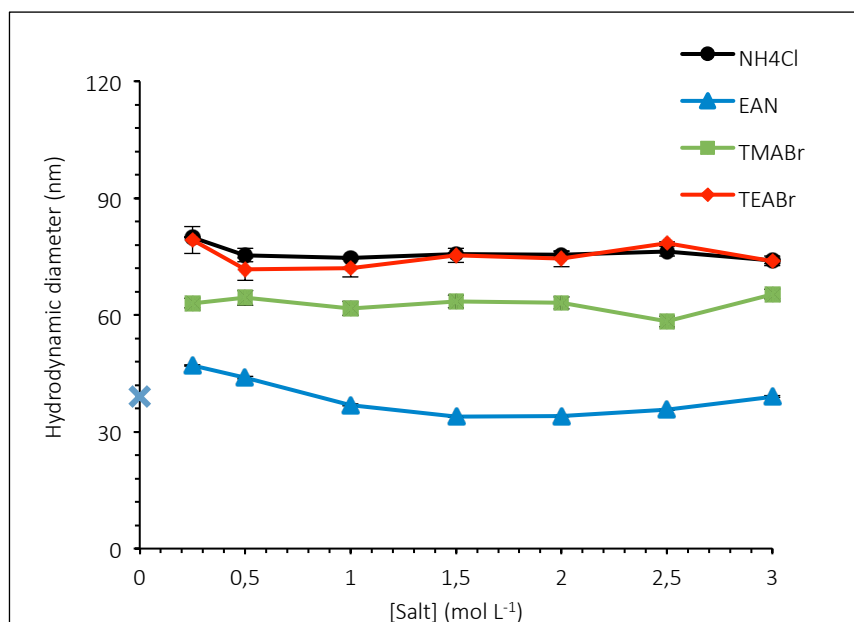


**Figure 2.** Hydrodynamic diameters of CNP in different aqueous solutions of  $\text{NH}_4\text{Cl}$ , EAN, TMABr and TEABr following a dilution pathway from 3 to  $\sim 0.2 \text{ mol L}^{-1}$  at a constant pH of 9.0. The size of CNP in pure water is marked as a Blue Cross. The initial concentration of CNPs in solution was 0.5 wt %. The

error bars come from standard deviation of multiple measurements at each point and in most cases, they are smaller than the symbols.

For the characterisation of electrostatic interactions of various mixtures, hydrodynamic size and UV-absorption measurements of samples were performed. As described previously, PAA-coated nanoparticles prepared and stored in water were used for all the mixtures. Their initial hydrodynamic diameter is 39 nm at 0.5 wt % in distilled water at pH 9.0. First, the hydrodynamic diameter of CNPs was measured at various concentrations of different salts to verify their stability without PC (Figure 2). Solutions of CNPs at 0.5 wt % were prepared in aqueous salt solutions of  $\text{NH}_4\text{Cl}$ , EAN, TMABr and TEABr. The initial aqueous salt solutions ( $c_{\text{salt}} = 3 \text{ mol L}^{-1}$ ;  $c_{\text{CNP}} = 0.5 \text{ wt } \%$ ) were diluted with distilled water step by step and the hydrodynamic diameter was measured, while maintaining an overall pH 9.0. Firstly, for the initial solutions ( $c_{\text{salt}} = 3 \text{ mol L}^{-1}$ ) we do observe an increase of the hydrodynamic diameter of the CNPs depending on the nature of the salt in solution. Only in the case of EAN, do we recover the hydrodynamic radius of CNPs in pure water. Therefore, some partial CNP aggregation takes place in the presence of  $\text{NH}_4\text{Cl}$ , TMABr and TEABr to begin with. Secondly, and more importantly, for any given salt, the hydrodynamic diameter of CNPs does not change over the whole dilution range indicating that the (partially aggregated) CNPs were stable in the range of 3 down to  $\sim 0.2 \text{ mol L}^{-1}$ , whatever the nature of the salt. Indeed, despite the presence of high concentration of salts, which in general induces electrostatic screening between charges on the PAA chains and hence a collapse of the polymer brush<sup>56,57</sup>, here the CNPs were well dispersed due electrostatic and steric repulsion.<sup>58</sup>

## 2.2 Coated maghemite nanoparticles in the presence of polycations in salt-free aqueous solutions

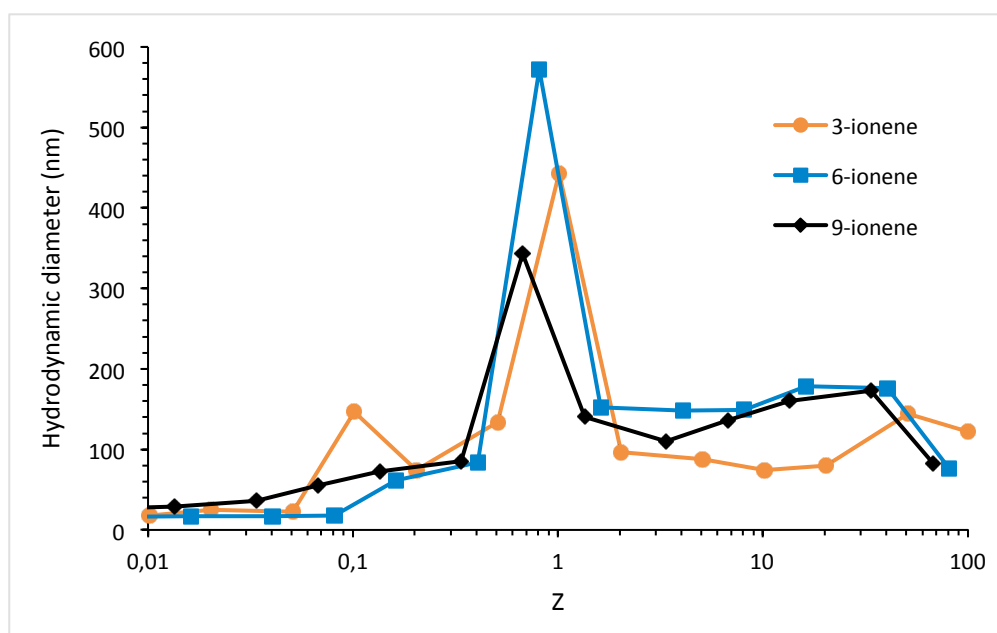


**Figure 3.** Hydrodynamic diameter of aggregates in mixtures of x-ionene (x=3, 6, 9) and CNPs as a function of the charge ratio  $Z = Z^+/Z^-$  at pH 9.0.

Hydrodynamic diameter of aggregates in mixtures of ionenes (3-, 6- and 9-ionene) and CNPs as a function of the charge ratio  $Z$  ( $Z = Z^+/Z^-$ ) are shown in Figure 3.  $Z$  is the charge ratio between the positively charged PCs ( $Z^+$ ) and the negatively charged CNPs ( $Z^-$ ). At  $Z = 1$ , we expect and indeed observe the largest aggregates (340-570 nm) in case of all ionenes, a stoichiometric compensation of the opposite charges is achieved at this charge ratio. For very small values of  $Z$  ( $Z \ll 1$ , excess of CNPs) we approach the hydrodynamic size of CNPs at 0.05 wt % in distilled water (measured as 22 nm). In this low-ionene limit, the majority of CNPs are well dispersed. For large values of  $Z$  ( $Z \gg 1$ , excess of ionenes) the hydrodynamic size oscillates between 70-160nm. Thus more extended aggregation is observed in this high-ionene limit, due to co-assembly of available CNPs with the PCs.<sup>22</sup> For the study of CNP-ionene mixtures in salty aqueous solutions, we chose to work at a slight excess of ionenes ( $Z$  slightly greater than 1) to ensure that all CNPs are involved in aggregation but at the same time avoiding the  $Z=1$  region, for which size determination by DLS becomes very inaccurate due to large aggregates formed.

### 2.3 Coated maghemite nanoparticles in the presence of polycations in salty aqueous solutions

To study the electrostatic interactions between coated maghemite nanoparticles and ionene polycations in the presence of different salts, mixtures of CNPs and 3-, 6- and 9-ionenes were prepared at charge ratios  $Z$  ( $Z = Z^+/Z^-$ ) of 5.1, 4.1 and 3.4 respectively, in 3 mol L<sup>-1</sup> aqueous salt solutions of NH<sub>4</sub>Cl, EAN, TMABr and TEABr in turn. These concentrated mixtures were then diluted stepwise with distilled water and characterized with DLS (Figure 4). To verify the dispersion state of the CNPs during the dilution process, the hydrodynamic diameter was compared to the values in Figure 2, which features the CNP behaviour in the respective aqueous salt solutions *in the absence of polycations*.

The experimental data confirms that CNPs in all the CNP-PC mixtures in 3 mol L<sup>-1</sup> aqueous salt solutions of NH<sub>4</sub>Cl, EAN, TMABr and TEABr are well dispersed prior to the dilution process. As dilution proceeds, at a given concentration of salt, called  $[\text{Salt}]_{\text{critical}}$ , a drastic increase in the hydrodynamic diameter of the CNPs is observed for each CNP-PC mixture, indicating the onset of aggregation between the oppositely charged CNPs and PCs. The sudden increase in the hydrodynamic diameter of the particles was observed both via the light scattering method as well as UV-Spectroscopy (3-ionene, SI 7). The  $[\text{Salt}]_{\text{critical}}$  values from Figure 4 are listed in Table 2.

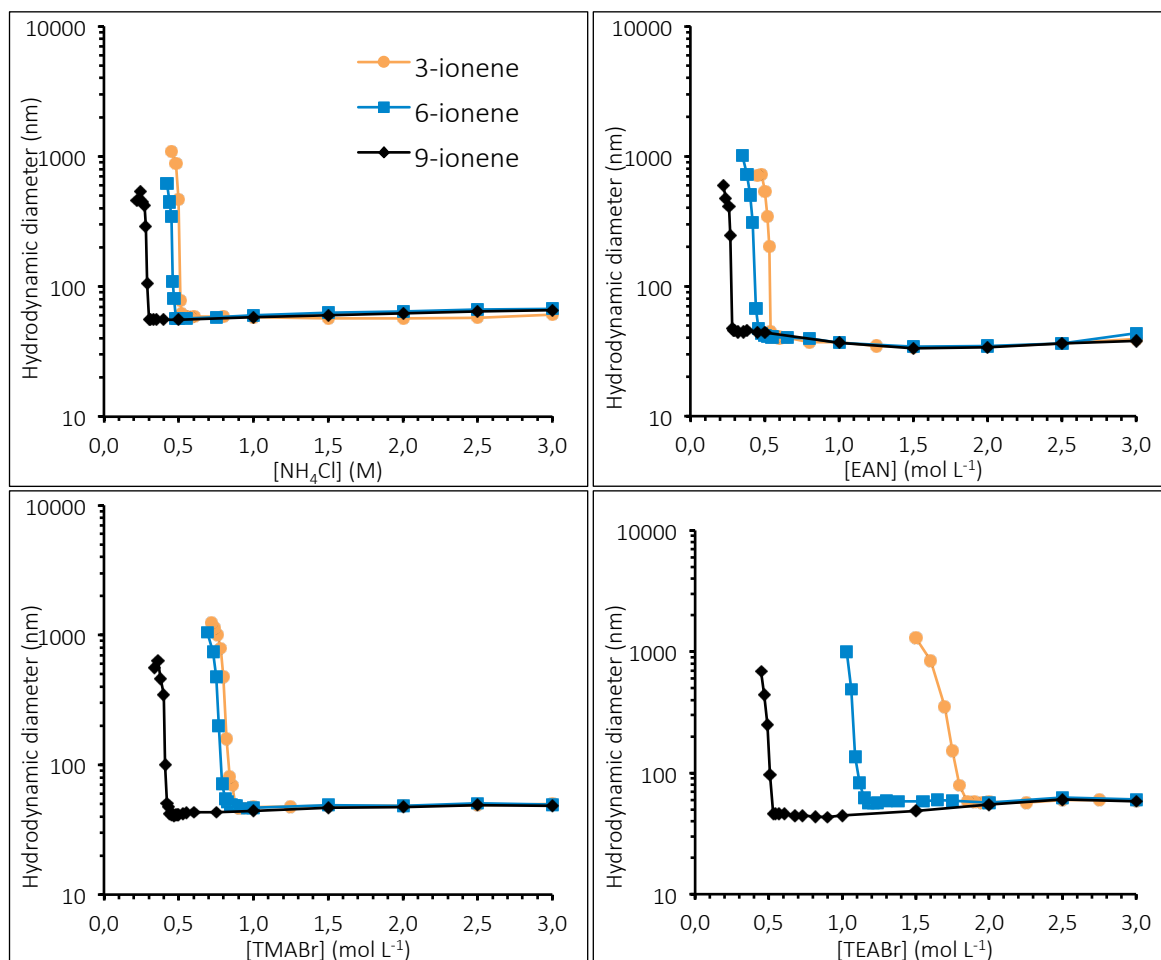


**Figure 4.** Dependence of the hydrodynamic diameter of CNPs in their mixtures with x-ionene (x=3, 6, or 9) PCs as a function of the salt concentration, for four different salts:  $\text{NH}_4\text{Cl}$ , EAN, TMABr and TEABr. CNPs and PCs were prepared at initial concentrations of 0.5 wt % at charge ratios Z ( $Z = Z^+/Z^-$ ) 5.1, 4.1 and 3.4, respectively. The initial salt concentration was  $3 \text{ mol L}^{-1}$  in each case, the concentration was gradually decreased through a dilution process with distilled water, while pH was kept constant at 9.0.

**Table 2.** Critical Salt concentrations ( $[\text{Salt}]_{\text{critical}}$ ) for mixtures of CNPs with ionene PCs in different aqueous salt solutions, extracted from data in Figure 4.

$[\text{Salt}]_{\text{critical}} (\text{mol L}^{-1})$	$\text{NH}_4\text{Cl}$	EAN	TMABr	TEABr
3-ionene	$0.54 \pm 0.01$	$0.55 \pm 0.01$	$0.90 \pm 0.01$	$1.85 \pm 0.05$
6-ionene	$0.48 \pm 0.01$	$0.48 \pm 0.02$	$0.83 \pm 0.02$	$1.18 \pm 0.03$

9-ionene	$0.30 \pm 0.01$	$0.29 \pm 0.01$	$0.47 \pm 0.01$	$0.53 \pm 0.02$
----------	-----------------	-----------------	-----------------	-----------------

The results allow to state that  $[\text{Salt}]_{\text{critical}}$  values depend strongly both on the charge density of the ionene polycation and the nature of the salt present. For all four salts,  $[\text{Salt}]_{\text{critical}}$  increases with increasing polycation charge density (even for modified I3-Bz ionene, SI 8). Regarding the nature of salt, we suggest it is the nature of the salt cation, as opposed to the salt anion, that is crucial in tuning the  $[\text{Salt}]_{\text{critical}}$ . In line with this, note that for TMABr and TEABr salts (different cations with the same bromide anion), the  $[\text{Salt}]_{\text{critical}}$  values increase significantly for all ionenes. In the mixtures, there is an excess of the ionenes ( $Z > 1$ ) and thus we depart from the picture of salt cations and positive charges on the polycation competing for the complexation with the negatively charged PAA-coated maghemite nanoparticles. The four salt cations considered are all based on an ammonium ion with a varying degree of hydrophobicity, according to the number and length of alkyl chains attached to the ammonium ions. In a simple first approach, these ions can be ordered in terms of their size, which reflects in broad terms also their hydration enthalpy and thus is a pertinent parameter to consider, as shall be seen from the following discussion. In Figure 5, the  $[\text{Salt}]_{\text{critical}}$  values are plotted as a function of the molar volumes of the four salt cations ( $V_{\text{cation}}$ , SI 4), determined on the basis of Millero et al.<sup>59</sup> This representation highlights two facts: (1) for a given PC charge density, mixtures with larger salt cations feature higher values of  $[\text{Salt}]_{\text{critical}}$ , in other words, the transition from a dispersed to an aggregated state along the dilution pathways occurs earlier; (2) mixtures with larger salt cations are increasingly more sensitive to the PC charge density. Overall, the worst combination for maintaining a well-dispersed CNP-PC mixture is the use of a salt with large cations in the presence of a densely charged PC.

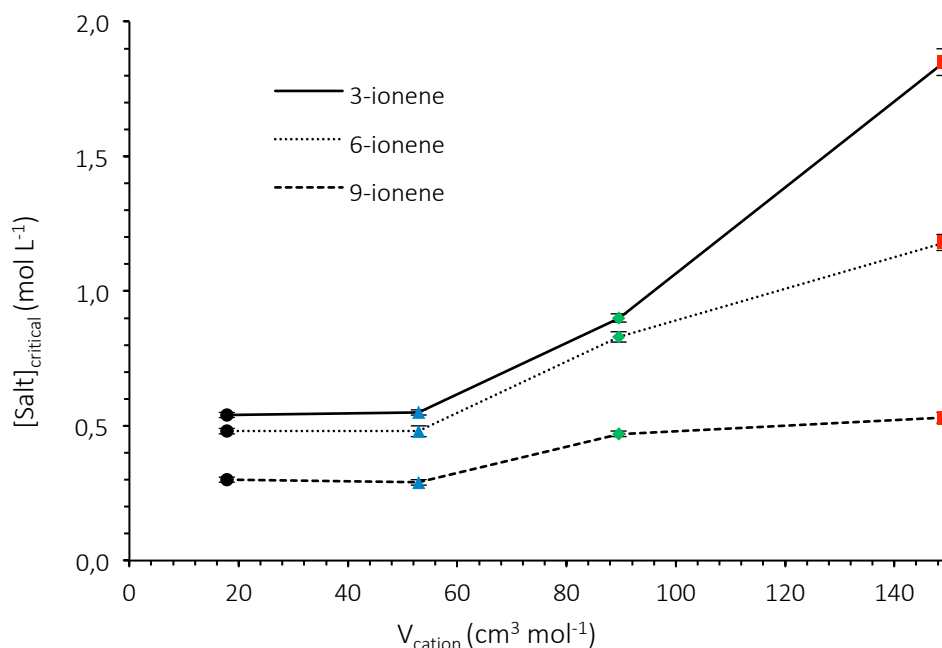


**Figure 5.** Critical salt concentration ( $[\text{Salt}]_{\text{critical}}$ ) values for mixtures derived from Figure 4 as a function of molar volume of salt cations ( $V_{\text{cation}}$ ). Transition values for 3- (full line), 6- (dotted line) and 9-ionene (dashed line) in different aqueous salt solutions:  $\text{NH}_4\text{Cl}$  (blue triangle), EAN (black round), TMABr (green diamond) and TEABr (red square).

We go now a step further and combine the two parameters (volume of salt cation and PC charge density), in search of a simple relationship to  $[\text{Salt}]_{\text{critical}}$ . If salt cation size (or volume) seems to be a critical parameter, the charge density of the polycation can be reconsidered in terms of a volume. For ionene polycations with tunable and perfectly regular charge distribution along the chain backbone<sup>44,45</sup>, it is trivial to express the charge density in terms of a volume per unit of charge (denoted here  $V_{\text{mono}}^+$ ). The higher the chain charge density, the lower the volume per unit of charge. In Figure 6,  $[\text{Salt}]_{\text{critical}}$  is expressed as a function of the ratio  $V_{\text{cation}}/V_{\text{mono}}^+$  and a simple linear dependence emerges. For completeness, the best linear fit of the entire data set leads to  $[\text{Salt}]_{\text{critical}} = 1.2 \frac{V_{\text{cation}}}{V_{\text{mono}}^+}$ . The molar volumes used for the salt cations and PC monomer units are summarised in SI 4 and SI 9. All data presented so far for PAA-coated maghemite NPs and ionene PCs are featured in Figure 6, together with additional data points available from supplementary measurements and the literature. The compound 3-Bz, also an ionene, was measured with CNPs in EAN and TMABr, with critical values of  $0.71 \pm 0.01$  and  $1.75 \pm 0.02 \text{ mol L}^{-1}$ , respectively (SI 8). The dramatic differences in the critical salt concentrations compared to 3-ionene can be contributed to  $\pi$ -stacking of the benzyl-group present in 3-Bz, but absent in 3-ionene. The PCs PTEA-PAM and PDADMAC mixed with PAA coated cerium oxide nanoparticles ( $\text{CeO}_2$ ) (equivalent electrosteric

behaviour to maghemite nanoparticles) produce according to literature transitions at 0.37 and 0.54 mol L<sup>-1</sup> NH<sub>4</sub>Cl, respectively.<sup>5</sup>

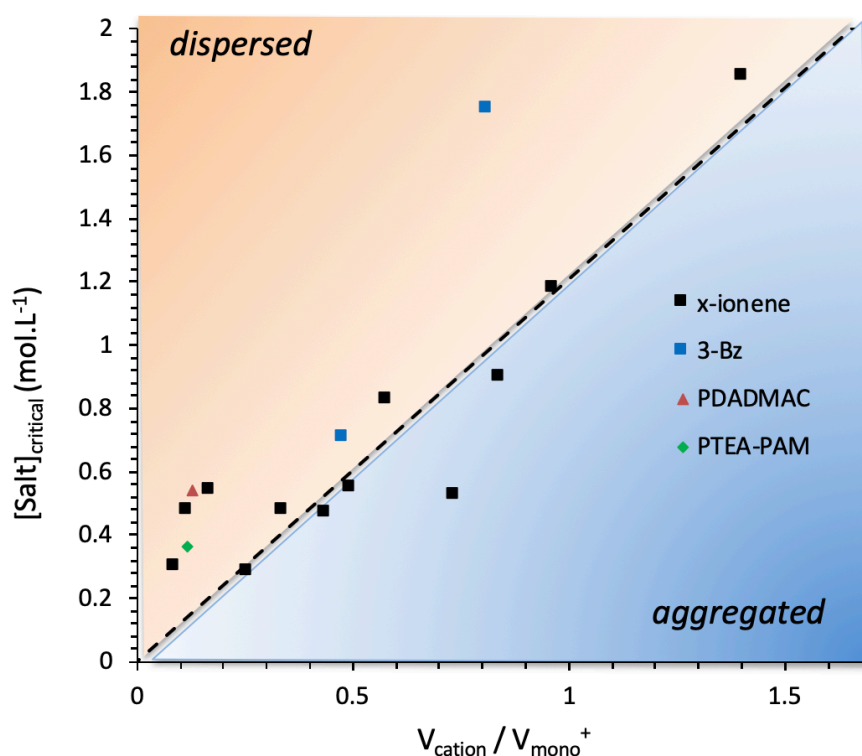


**Figure 6.**  $[\text{Salt}]_{\text{critical}}$  plotted as a function of the ratio  $V_{\text{cation}}/V_{\text{mono}}^+$  for all data presented in Figure 5 (“x-ionene” data series), together with additional data from supplementary measurements and the literature.  $[\text{Salt}]_{\text{critical}}$  is the critical salt concentration at which aggregation of PAA-coated nanoparticles in the presence of polycations appears,  $V_{\text{cation}}$  is the molar volume of salt cations and  $V_{\text{mono}}^+$  is the average molar volume per charged monomer unit of the polycation (SI 4 and SI 9). The dashed line is the linear fit of all the  $[\text{Salt}]_{\text{critical}}$  values for ionenes.

The master curve in Figure 6 seems to be a very simple tool for designing a system with a desired  $[\text{Salt}]_{\text{critical}}$ . The critical salt concentration is proportional to the ratio of volumes of the salt cation and the polycation monomer. The passage of the master curve through the origin corresponds to the zero salt case, for which an aggregated state is observed. In order to understand the appearance of the master curve we start with a picture based on the competition of these two species in the complexation with the PAA brush of the CNPs. The reason why the size of the monomer is considered



here is related to the high salt concentration, for which no Debye Length can be defined (smaller than the size of a single atom). Although the structure of the polymer chain has a role on the particle aggregation, the local interactions are considered at the level of the monomer unit.

Let us consider at first the effect of size and hydration of salts, as Collins and coworkers did<sup>32,60</sup>. The point developed in Collins's models derives from the impossibility to describe the local effect of salt from classical mean field theory, and especially at high salt concentration. Collins uses the classical ordering of salts dealing with their ability to balance preferentially their interactions with water molecules (kosmotropes) or with their counterion (chaotropes). Further, Collins reports on the affinity for two oppositely charged kosmotropes to make ions pairs, as well as two chaotropes, but low probability of ion pairing for chaotrope-kosmotrope pairs. These considerations are at the origin of the phase separation in mixture of two anions ( $\text{Cl}^-$  and  $\text{TFSi}^-$ ) sharing the same cation ( $\text{Li}^+$ )<sup>61</sup>. Kosmotropes are described as small highly charged ions (carboxylate anions, characterized by a molar volume of  $43.6 \text{ cm}^3 \cdot \text{mol}^{-1}$ , in the present system) and chaotropes as large and weakly charged ions (ammonium cations in the present system).<sup>32</sup> Considering our system, the cations are ranging from  $\text{NH}_4^+$  to  $\text{TEA}^+$ , with increasing size ranging from  $\text{NH}_4^+$  ( $17.86 \text{ cm}^3 \cdot \text{mol}^{-1}$ ),  $\text{EA}^+$  ( $52.94 \text{ cm}^3 \cdot \text{mol}^{-1}$ ),  $\text{TMA}^+$  ( $89.57 \text{ cm}^3 \cdot \text{mol}^{-1}$ ), and to  $\text{TEA}^+$  ( $149.12 \text{ cm}^3 \cdot \text{mol}^{-1}$ ), thus a more pronounced chaotropic behavior. The determination of the Jones-Dole viscosity B coefficient was achieved from the variation of viscosity of salt solution, for salt concentration ranging from  $0.5 \text{ mol} \cdot \text{L}^{-1}$  to  $3 \text{ mol} \cdot \text{L}^{-1}$  (figure SI-10). The global trend shows that the larger the size of the counterion, the larger the Jones-Dole viscosity B coefficient, which confirms the increasingly chaotropic behavior along the above cation series.

Our conceptual picture behind the representation in Figure 6, is based on salt cations competing with monomer units of the polycation for complexation to the PAA-coating and the relative volumes of the two competitors are being decisive. The  $V_{\text{cation}}/V_{\text{mono}}^+$  ratio is an important parameter if we consider it under the ion-pairing scheme proposed by Collins and coworkers<sup>32</sup>: oppositely charged species with similar sizes have a stronger ion binding tendency than those with dissimilar size. Under the Collins scheme, carboxylate ions are considered as small kosmotropic anions and thus of favourable ion pairing with the small cations of the series considered,  $\text{NH}_4^+$  and  $\text{EA}^+$ , and less so as the  $V_{\text{cation}}$  increases, case of  $\text{TMA}^+$  and  $\text{TBA}^+$ . The ratio  $V_{\text{cation}}/V_{\text{mono}}^+$  thus reflects the *relative* ion-pairing tendency of the PAA carboxylate group with the salt cation on one side and the monomer of the polycation on the other: the higher the  $V_{\text{cation}}/V_{\text{mono}}^+$  ratio, the more favourable is the “polycation-PAA” pairing relative to “salt cation-PAA” pairing. The more favourable the polycation-PAA pairing, the wider is the salt concentration range over which aggregation is seen, i.e. the higher is the critical salt concentration or the aggregation threshold. For a given salt type, the

increase of the polycation (ionene) monomer size (from 3-ionene to 9-ionene) leads to a decrease in  $[\text{Salt}]_{\text{critical}}$ , as the ionene-PAA pairing is increasingly unfavorable.

At this point, it is interesting to link the above picture with that developed by Schlenoff et al<sup>39</sup>, based on salt ions “doping” a polycation-polyanion complex and ultimately dissolving the complex for high degrees of such doping. By using the Collins concept based on “matching” ion sizes, we have constructed a way to express the degree of “doping” by salt ions in the form of the  $V_{\text{cation}}/V_{\text{mono}}^+$  ratio. As  $V_{\text{cation}}/V_{\text{mono}}^+$  increases (moving along a horizontal line from left to right in Figure 6) the degree of salt doping decreases, polycation-polyanion complexation is more favourable and a transition from a dispersed to an aggregated state is observed. From the Schlenoff point of view, it is more natural to consider a decreasing  $V_{\text{cation}}/V_{\text{mono}}^+$  (right to left in Figure 6), which is accompanied by an increase in salt “doping” and a transition from a polyelectrolyte complex (called here “aggregated” state) to a dissolved polyelectrolyte complex (here “dispersed” state) is observed.

### 3 CONCLUSIONS

In conclusion, we provide here a simple tool for tuning the dispersed-aggregated transition in salty aqueous solutions of PAA-coated NPs in the presence of polycations. This tuning is achieved via a combination of two parameters: volume of the salt cation ( $V_{\text{cation}}$ ) and volume of the charged monomer unit of the polycation ( $V_{\text{mono}}^+$ , reflecting the polycation charge density). The critical salt concentration, corresponding to the dispersed-aggregated transition of the NPs, follows in a linear fashion the ratio of the above two volumes,  $V_{\text{cation}}/V_{\text{mono}}^+$ . The higher the  $V_{\text{cation}}/V_{\text{mono}}^+$  ratio, the narrower the region of dispersed NP state at high salt concentration, i.e. the earlier take place the onset of aggregation as the system is diluted from the high salt concentration limit. In other words, the worst combination for maintaining a well-dispersed NP-PC mixture over a wide salt concentration range is the use of a salt with large cations in the presence of a densely charged polycation (small  $V_{\text{mono}}^+$ ). The master curve was built from a data set of PAA-coated maghemite nanoparticles in the presence of linear polycations (ionenes) and salt cations both based on ammonium charged centres, supplemented by a few neighbouring systems. A generalisation of the master curves to other types of cations and polycations necessarily involves consideration going beyond that of ion size, and their position in the Hofmeister series is the best existing, albeit empirical, starting point.

Phenomena at high salt concentrations are at play and the conceptual picture rationalizing the observed master curve focuses on local ion-pairing tendencies of the species involved. The central idea is that salt cations and polycation monomers compete in the complexation with the polyanion brush on the nanoparticles. The originality comes from using the Collins concept based on

“matching” ion sizes, to express, via the  $V_{\text{cation}}/V_{\text{mono}}^+$  ratio, the *relative* ion-pairing tendency of the polyanion group with the salt cation on one side and the monomer of the polycation on the other. The higher the  $V_{\text{cation}}/V_{\text{mono}}^+$  ratio, the more favourable is the “polycation-PAA” pairing relative to “salt cation-PAA” pairing. This simple concept rationalizes the ensemble of the observed aggregation thresholds and highlights the importance of local ion-pairing phenomena in polyion complexation, governing here the aggregation of polymer-coated nanoparticles. Our approach leads successfully to a master curve predicting the phase diagram of polymer-coated magnetic nanoparticles.

## 4 Acknowledgements

Authors wish to acknowledge Yasmina Bouharicha for her assistance during benzylic ionene synthesis and Aude Michel-Tourgis for the synthesis of iron oxide nanoparticles.

## 5 REFERENCES

- (1) Cazares-Cortes, E.; Cabana, S.; Boitard, C.; Nehlig, E.; Griffete, N.; Fresnais, J.; Wilhelm, C.; Abou-Hassan, A.; Ménager, C. Recent Insights in Magnetic Hyperthermia: From the “Hot-Spot” Effect for Local Delivery to Combined Magneto-Photo-Thermia Using Magneto-Plasmonic Hybrids. *Advanced Drug Delivery Reviews* **2019**, *138*, 233–246. <https://doi.org/10.1016/j.addr.2018.10.016>.
- (2) Chanana, M.; Mao, Z.; Wang, D. Using Polymers to Make Up Magnetic Nanoparticles for Biomedicine. *Journal of Biomedical Nanotechnology* **2009**, *5* (6), 652–668. <https://doi.org/10.1166/jbn.2009.1082>.
- (3) Peng, E.; Wang, F.; Xue, J. M. Nanostructured Magnetic Nanocomposites as MRI Contrast Agents. *J. Mater. Chem. B* **2015**, *3* (11), 2241–2276. <https://doi.org/10.1039/C4TB02023E>.
- (4) Hugounenq, P.; Levy, M.; Alloyeau, D.; Lartigue, L.; Dubois, E.; Cabuil, V.; Ricolleau, C.; Roux, S.; Wilhelm, C.; Gazeau, F.; Bazzi, R. Iron Oxide Monocrystalline Nanoflowers for Highly Efficient Magnetic Hyperthermia. *Journal of Physical Chemistry C* **2012**, *116* (29), 15702–15712. <https://doi.org/10.1021/jp3025478>.
- (5) Yan, M.; Fresnais, J.; Sekar, S.; Chapel, J.-P.; Berret, J.-F. Magnetic Nanowires Generated via the Waterborne Desalting Transition Pathway. *ACS Appl. Mater. Interfaces* **2011**, *3* (4), 1049–1054. <https://doi.org/10.1021/am101188y>.
- (6) Harada, A.; Kataoka, K. Chain Length Recognition: Core-Shell Supramolecular Assembly from Oppositely Charged Block Copolymers. *Science* **1999**, *283* (5398), 65–67. <https://doi.org/10.1126/science.283.5398.65>.
- (7) Leclercq, L.; Boustta, M.; Vert, M. A Physico-Chemical Approach of Polyanion-Polycation Interactions Aimed at Better Understanding the In Vivo Behaviour of Polyelectrolyte-Based Drug Delivery and Gene Transfection. *Journal of Drug Targeting* **2003**, *11* (3), 129–138. <https://doi.org/10.1080/1061186031000150287>.
- (8) Campbell, A. I.; Anderson, V. J.; van Duijneveldt, J. S.; Bartlett, P. Dynamical Arrest in Attractive Colloids: The Effect of Long-Range Repulsion. *Phys. Rev. Lett.* **2005**, *94* (20), 208301. <https://doi.org/10.1103/PhysRevLett.94.208301>.

- (9) Leunissen, M. E.; Christova, C. G.; Hynninen, A.-P.; Royall, C. P.; Campbell, A. I.; Imhof, A.; Dijkstra, M.; Roij, R. van; Blaaderen, A. van. Ionic Colloidal Crystals of Oppositely Charged Particles. *Nature* **2005**, *437* (7056), 235–240. <https://doi.org/10.1038/nature03946>.
- (10) Etrych, T.; Leclercq, L.; Boustta, M.; Vert, M. Polyelectrolyte Complex Formation and Stability When Mixing Polyanions and Polycations in Salted Media: A Model Study Related to the Case of Body Fluids. *European Journal of Pharmaceutical Sciences* **2005**, *25* (2), 281–288. <https://doi.org/10.1016/j.ejps.2005.03.005>.
- (11) Ulrich, S.; Seijo, M.; Stoll, S. The Many Facets of Polyelectrolytes and Oppositely Charged Macroions Complex Formation. *Current Opinion in Colloid & Interface Science* **2006**, *11* (5), 268–272. <https://doi.org/10.1016/j.cocis.2006.08.002>.
- (12) Hales, K.; Pochan, D. J. Using Polyelectrolyte Block Copolymers to Tune Nanostructure Assembly. *Current Opinion in Colloid & Interface Science* **2006**, *11* (6), 330–336. <https://doi.org/10.1016/j.cocis.2006.12.004>.
- (13) Krotova, M. K.; Vasilevskaya, V. V.; Leclercq, L.; Boustta, M.; Vert, M.; Khokhlov, A. R. Salt Effects on Complexes of Oppositely Charged Macromolecules Having Different Affinity to Water. *Macromolecules* **2009**, *42* (19), 7495–7503. <https://doi.org/10.1021/ma900204u>.
- (14) Massart, R. Preparation of Aqueous Magnetic Liquids in Alkaline and Acidic Media. *IEEE Transactions on Magnetics* **1981**, *17* (2), 1247–1248. <https://doi.org/10.1109/TMAG.1981.1061188>.
- (15) Bee, A.; Massart, R.; Neveu, S. Synthesis of Very Fine Maghemite Particles. *Journal of Magnetism and Magnetic Materials* **1995**, *149* (1), 6–9. [https://doi.org/10.1016/0304-8853\(95\)00317-7](https://doi.org/10.1016/0304-8853(95)00317-7).
- (16) Lefebure, S.; Dubois, E.; Cabuil, V.; Neveu, S.; Massart, R. Monodisperse Magnetic Nanoparticles: Preparation and Dispersion in Water and Oils. *Journal of Materials Research* **1998**, *13* (10), 2975–2981. <https://doi.org/10.1557/JMR.1998.0407>.
- (17) Lucas, I. T.; Durand-Vidal, S.; Dubois, E.; Chevalet, J.; Turq, P. Surface Charge Density of Maghemite Nanoparticles: Role of Electrostatics in the Proton Exchange. *J. Phys. Chem. C* **2007**, *111* (50), 18568–18576. <https://doi.org/10.1021/jp0743119>.
- (18) Fresnais, J.; Yan, M.; Courtois, J.; Bostelmann, T.; Bée, A.; Berret, J.-F. Poly(Acrylic Acid)-Coated Iron Oxide Nanoparticles: Quantitative Evaluation of the Coating Properties and Applications for the Removal of a Pollutant Dye. *Journal of Colloid and Interface Science* **2013**, *395*, 24–30. <https://doi.org/10.1016/j.jcis.2012.12.011>.
- (19) Biggs, S.; Healy, T. W. Electrosteric Stabilisation of Colloidal Zirconia with Low-Molecular-Weight Polyacrylic Acid. An Atomic Force Microscopy Study. *J. Chem. Soc., Faraday Trans.* **1994**, *90* (22), 3415–3421. <https://doi.org/10.1039/FT9949003415>.
- (20) Sehgal, A.; Lalatonne, Y.; Berret, J.-F.; Morvan, M. Precipitation–Redispersion of Cerium Oxide Nanoparticles with Poly(Acrylic Acid): Toward Stable Dispersions. *Langmuir* **2005**, *21* (20), 9359–9364. <https://doi.org/10.1021/la0513757>.
- (21) Guibert, C.; Dupuis, V.; Peyre, V.; Fresnais, J. Hyperthermia of Magnetic Nanoparticles: Experimental Study of the Role of Aggregation. *J. Phys. Chem. C* **2015**, *119* (50), 28148–28154. <https://doi.org/10.1021/acs.jpcc.5b07796>.
- (22) Fresnais, J.; Lavelle, C.; Berret, J.-F. Nanoparticle Aggregation Controlled by Desalting Kinetics. *J. Phys. Chem. C* **2009**, *113* (37), 16371–16379. <https://doi.org/10.1021/jp904665u>.
- (23) van der Burgh, S.; de Keizer, A.; Cohen Stuart, M. A. Complex Coacervation Core Micelles.

- Colloidal Stability and Aggregation Mechanism. *Langmuir* **2004**, *20* (4), 1073–1084. <https://doi.org/10.1021/la035012n>.
- (24) Voets, I. K.; de Keizer, A.; Cohen Stuart, M. A.; Justynska, J.; Schlaad, H. Irreversible Structural Transitions in Mixed Micelles of Oppositely Charged Diblock Copolymers in Aqueous Solution. *Macromolecules* **2007**, *40* (6), 2158–2164. <https://doi.org/10.1021/ma0614444>.
- (25) Yadel, C.; Michel, A.; Casale, S.; Fresnais, J. Hyperthermia Efficiency of Magnetic Nanoparticles in Dense Aggregates of Cerium Oxide/Iron Oxide Nanoparticles. *Applied Sciences* **2018**, *8* (8), 1241. <https://doi.org/10.3390/app8081241>.
- (26) Ou, Z.; Muthukumar, M. Entropy and Enthalpy of Polyelectrolyte Complexation: Langevin Dynamics Simulations. *The Journal of Chemical Physics* **2006**, *124* (15), 154902. <https://doi.org/10.1063/1.2178803>.
- (27) Adhikari, S.; Leaf, M. A.; Muthukumar, M. Polyelectrolyte Complex Coacervation by Electrostatic Dipolar Interactions. *The Journal of Chemical Physics* **2018**, *149* (16), 163308. <https://doi.org/10.1063/1.5029268>.
- (28) Shi, L.; Carn, F.; Boué, F.; Mosser, G.; Buhler, E. Control over the Electrostatic Self-Assembly of Nanoparticle Semiflexible Biopolyelectrolyte Complexes. *Soft Matter* **2013**, *9* (20), 5004. <https://doi.org/10.1039/c3sm27138b>.
- (29) Delorme, N.; Bardeau, J. F.; Carriere, D.; Dubois, M.; Gourbil, A.; Mohwald, H.; Zemb, T.; Fery, A. Experimental Evidence of the Electrostatic Contribution to the Bending Rigidity of Charged Membranes. *Journal of Physical Chemistry B* **2007**, *111* (10), 2503–2505. <https://doi.org/10.1021/jp068252v>.
- (30) Tóth, I. Y.; Nesztor, D.; Novák, L.; Illés, E.; Szekeres, M.; Szabó, T.; Tombácz, E. Clustering of Carboxylated Magnetite Nanoparticles through Polyethylenimine: Covalent versus Electrostatic Approach. *Journal of Magnetism and Magnetic Materials* **2017**, *427*, 280–288. <https://doi.org/10.1016/j.jmmm.2016.11.011>.
- (31) Kunz, W. Specific Ion Effects in Colloidal and Biological Systems. *Current Opinion in Colloid & Interface Science* **2010**, *15* (1–2), 34–39. <https://doi.org/10.1016/j.cocis.2009.11.008>.
- (32) Collins, K. D. Why Continuum Electrostatics Theories Cannot Explain Biological Structure, Polyelectrolytes or Ionic Strength Effects in Ion–Protein Interactions. *Biophysical Chemistry* **2012**, *167*, 43–59. <https://doi.org/10.1016/j.bpc.2012.04.002>.
- (33) Salis, A.; Ninham, B. W. Models and Mechanisms of Hofmeister Effects in Electrolyte Solutions, and Colloid and Protein Systems Revisited. *Chem. Soc. Rev.* **2014**, *43* (21), 7358–7377. <https://doi.org/10.1039/C4CS00144C>.
- (34) Spruijt, E.; Bakker, H. E.; Kodger, T. E.; Sprakel, J.; Cohen Stuart, M. A.; van der Gucht, J. Reversible Assembly of Oppositely Charged Hairy Colloids in Water. *Soft Matter* **2011**, *7* (18), 8281. <https://doi.org/10.1039/c1sm05881a>.
- (35) Spruijt, E.; Westphal, A. H.; Borst, J. W.; Cohen Stuart, M. A.; van der Gucht, J. Binodal Compositions of Polyelectrolyte Complexes. *Macromolecules* **2010**, *43* (15), 6476–6484. <https://doi.org/10.1021/ma101031t>.
- (36) Salehi, A.; Larson, R. G. A Molecular Thermodynamic Model of Complexation in Mixtures of Oppositely Charged Polyelectrolytes with Explicit Account of Charge Association/Dissociation. *Macromolecules* **2016**, *49* (24), 9706–9719. <https://doi.org/10.1021/acs.macromol.6b01464>.
- (37) Limo, M. J.; Perry, C. C. Thermodynamic Study of Interactions Between ZnO and ZnO

- Binding Peptides Using Isothermal Titration Calorimetry. *Langmuir* **2015**, *31* (24), 6814–6822. <https://doi.org/10.1021/acs.langmuir.5b01347>.
- (38) Fu, J.; Fares, H. M.; Schlenoff, J. B. Ion-Pairing Strength in Polyelectrolyte Complexes. *Macromolecules* **2017**, *50* (3), 1066–1074. <https://doi.org/10.1021/acs.macromol.6b02445>.
- (39) Schlenoff, J. B.; Yang, M.; Digby, Z. A.; Wang, Q. Ion Content of Polyelectrolyte Complex Coacervates and the Donnan Equilibrium. *Macromolecules* **2019**, *52* (23), 9149–9159. <https://doi.org/10.1021/acs.macromol.9b01755>.
- (40) Olvera-de-la-Cruz, M.; Belloni, L.; Delsanti, M.; Dalbiez, J. P.; Spalla, O.; Drifford, M. Precipitation of Highly Charged Polyelectrolytes Solutions in Presence of Multivalent Salts. *J. Chem. Phys* **1995**, *103*, 5781–5791.
- (41) Muthukumar, M. *50th Anniversary Perspective*: A Perspective on Polyelectrolyte Solutions. *Macromolecules* **2017**, *50* (24), 9528–9560. <https://doi.org/10.1021/acs.macromol.7b01929>.
- (42) Rathee, V. S.; Sidky, H.; Sikora, B. J.; Whitmer, J. K. Role of Associative Charging in the Entropy–Energy Balance of Polyelectrolyte Complexes. *J. Am. Chem. Soc.* **2018**, *140* (45), 15319–15328. <https://doi.org/10.1021/jacs.8b08649>.
- (43) Massart, R. Preparation of Aqueous Magnetic Liquids in Alkaline and Acidic Media. *IEEE Transactions on Magnetics* **1981**, *17* (2), 1247–1248. <https://doi.org/10.1109/TMAG.1981.1061188>.
- (44) Malikova, N.; Čebašek, S.; Glenisson, V.; Bhowmik, D.; Carrot, G.; Vlachy, V. Aqueous Solutions of Ionenenes: Interactions and Counterion Specific Effects as Seen by Neutron Scattering. *Phys. Chem. Chem. Phys.* **2012**, *14* (37), 12898–12904. <https://doi.org/10.1039/C2CP41859B>.
- (45) Malikova, N.; Rollet, A.-L.; Cebasek, S.; Tomsic, M.; Vlachy, V. On the Crossroads of Current Polyelectrolyte Theory and Counterion-Specific Effects. *Phys. Chem. Chem. Phys.* **2015**, *17* (8), 5650–5658. <https://doi.org/10.1039/C4CP05469E>.
- (46) Rembaum, A.; Noguchi, H. Reactions of N,N,N',N'-Tetramethyl- $\alpha,\iota$ -Diaminoalkanes with  $\alpha,\iota$ -Dihaloalkanes. II. x-y Reactions. *Macromolecules* **1972**, *5* (3), 261–269. <https://doi.org/10.1021/ma60027a007>.
- (47) Layman, J. M.; Borgerding, E. M.; Williams, S. R.; Heath, W. H.; Long, T. E. Synthesis and Characterization of Aliphatic Ammonium Ionenenes: Aqueous Size Exclusion Chromatography for Absolute Molecular Weight Characterization. *Macromolecules* **2008**, *41* (13), 4635–4641. <https://doi.org/10.1021/ma800549j>.
- (48) Michaels, A. S.; Morelos, O. Polyelectrolyte Adsorption by Kaolinite. *Ind. Eng. Chem.* **1955**, *47* (9), 1801–1809. <https://doi.org/10.1021/ie50549a029>.
- (49) Wiśniewska, M.; Chibowski, S. Influence of Temperature and Purity of Polyacrylic Acid on Its Adsorption and Surface Structures at the ZrO<sub>2</sub>/Polymer Solution Interface: *Adsorption Science & Technology* **2016**. <https://doi.org/10.1260/026361705775373279>.
- (50) Sakhawoth, Y.; Michot, L. J.; Levitz, P.; Malikova, N. Flocculation of Clay Colloids Induced by Model Polyelectrolytes: Effects of Relative Charge Density and Size. *ChemPhysChem* **2017**, *18* (19), 2756–2765. <https://doi.org/10.1002/cphc.201700430>.
- (51) Fedors, R. F. A Method for Estimating Both the Solubility Parameters and Molar Volumes of Liquids. *Polymer Engineering & Science* **1974**, *14* (2), 147–154. <https://doi.org/10.1002/pen.760140211>.
- (52) Evans, D. F.; Yamauchi, A.; Roman, R.; Casassa, E. Z. Micelle Formation in Ethylammonium

Nitrate, a Low-Melting Fused Salt. *J. Colloid Interface Sci.; (United States)* **1982**, *88*:1.  
[https://doi.org/10.1016/0021-9797\(82\)90157-6](https://doi.org/10.1016/0021-9797(82)90157-6).

(53) Mamusa, M.; Sirieix-Plénet, J.; Cousin, F.; Perzynski, R.; Dubois, E.; Peyre, V. Microstructure of Colloidal Dispersions in the Ionic Liquid Ethylammonium Nitrate: Influence of the Nature of the Nanoparticles' Counterion. *J. Phys.: Condens. Matter* **2014**, *26* (28), 284113.  
<https://doi.org/10.1088/0953-8984/26/28/284113>.

(54) Guibert, C.; Dupuis, V.; Fresnais, J.; Peyre, V. Controlling Nanoparticles Dispersion in Ionic Liquids by Tuning the PH. *Journal of Colloid and Interface Science* **2015**, *454*, 105–111.  
<https://doi.org/10.1016/j.jcis.2015.04.059>.

(55) The Iron Oxides. In *Iron Oxides in the Laboratory*; John Wiley & Sons, Ltd, 2007; pp 5–18.  
<https://doi.org/10.1002/9783527613229.ch01>.

(56) Akkilic, N.; de Vos, W. M. 5 - Responsive Polymer Brushes for Biomedical Applications. In *Switchable and Responsive Surfaces and Materials for Biomedical Applications*; Zhang, Z., Ed.; Woodhead Publishing: Oxford, 2015; pp 119–146. <https://doi.org/10.1016/B978-0-85709-713-2.00005-5>.

(57) Ballauff, M.; Borisov, O. Polyelectrolyte Brushes. *Current Opinion in Colloid & Interface Science* **2006**, *11* (6), 316–323. <https://doi.org/10.1016/j.cocis.2006.12.002>.

(58) Currie, E. P. K.; Sieval, A. B.; Fleer, G. J.; Stuart, M. A. C. Polyacrylic Acid Brushes: Surface Pressure and Salt-Induced Swelling. *Langmuir* **2000**, *16* (22), 8324–8333.  
<https://doi.org/10.1021/la991528o>.

(59) Millero, F. J. Molal Volumes of Electrolytes. *Chem. Rev.* **1971**, *71* (2), 147–176.  
<https://doi.org/10.1021/cr60270a001>.

(60) Collins, K. D. Charge Density-Dependent Strength of Hydration and Biological Structure. *Biophysical Journal* **1997**, *72* (1), 65–76. [https://doi.org/10.1016/S0006-3495\(97\)78647-8](https://doi.org/10.1016/S0006-3495(97)78647-8).

(61) Dubouis, N.; Park, C.; Deschamps, M.; Abdelghani-Idrissi, S.; Kanduč, M.; Colin, A.; Salanne, M.; Dzubiella, J.; Grimaud, A.; Rotenberg, B. Chasing Aqueous Biphasic Systems from Simple Salts by Exploring the LiTFSI/LiCl/H<sub>2</sub>O Phase Diagram. *ACS Cent. Sci.* **2019**, *5* (4), 640–643. <https://doi.org/10.1021/acscentsci.8b00955>.